Dynamics of a semiconductor laser with feedback and modulation: experiments and model comparison

JORDI TIANA-ALSINA[1] AND CRISTINA MASOLLER[2,*]

[1]*Department de Física Aplicada, Facultat de Fisica, Universitat de Barcelona, Marti i Franques 1, 08028 Barcelona, Spain*
[2]*Departament de Fisica, Universitat Politecnica de Catalunya, Rambla Sant Nebridi 22, 08222 Terrassa, Barcelona, Spain*
*cristina.masoller@upc.edu

Abstract: We study experimentally and numerically the dynamics of a semiconductor laser near threshold, subject to optical feedback and sinusoidal current modulation. The laser operates in the low frequency fluctuation (LFF) regime where, without modulation, the intensity shows sudden spikes at irregular times. Under particular modulation conditions the spikes lock to the modulation and their timing becomes highly regular. While the modulated LFF dynamics has received a lot of attention, an in-depth comparison with the predictions of the Lang-Kobayashi (LK) model has not yet been performed. Here we use the LK model to simulate the laser dynamics and use the Fano factor to quantify the regularity of the timing of the spikes. The Fano factor is calculated by counting the number of spikes in successive segments of the intensity time-series and keeps information about temporal order in the spike sequence that is lost when the analysis is based on the distribution of inter-spike intervals. Here we compare the spike timing regularity in experimental and in simulated spike sequences as a function of the modulation amplitude and frequency and find a good qualitative agreement. We find that in both experiments and simulation for appropriate conditions the spike timing can be highly regular, as revealed by very small values of the Fano factor.

1. Introduction

The nonlinear dynamics of semiconductor lasers with optical feedback has attracted attention over many years. It is well-known that the interplay of oscillations of different frequencies (the relaxation oscillation frequency, the mode beat frequency, the mode switching frequency, the external-cavity frequency, and the current modulation frequency) can give rise to a rich variety of nonlinear behaviors [1–13].

Close to threshold (in the so-called low-frequency fluctuations, LFF, regime) and without current modulation, the laser intensity shows sudden spikes that occur at irregular times, with an average spike rate in the MHz range. Under low-frequency, small-amplitude sinusoidal modulation of the laser current (in the MHz range), the spikes lock to the modulation and tend to occur at intervals that are multiples of the modulation period [14–23].

The LFF dynamics is well represented by the Lang-Kobayashi (LK) model [24]. We have recently found experimentally [22] and numerically [25] that small-amplitude sinusoidal modulation (2-3% variation of the dc value of the laser current) can generate, for particular modulation frequencies, subharmonic locking, such that a spike is emitted with regular periodicity, every two or every three modulation cycles. In contrast, harmonic locking (such that the laser emits a spike every modulation cycle) was not found under small-amplitude sinusoidal modulation. Experimental studies and LK model simulations have found that harmonic locking can be achieved with larger modulation amplitude [10,14,25]; however, a systematic comparison of experiments

and model predictions, as a function of the modulation amplitude and frequency, is still lacking. Here, to fill this gap, we analyze experimental and simulated spike sequences, and use the Fano factor to characterize the role of the modulation amplitude and frequency in the regularity of the spike timing.

While we have uncovered temporal order in the sequence of inter-spike-intervals (ISIs) [19–21,23] by using the well-known symbolic method of ordinal analysis [26–28], this method only allowed us to detect correlations between a few ISIs. Specifically, by considering patterns of size $L = 3$ we uncovered correlations among three ISIs. Longer patterns could have been used but that would have required longer ISI sequences to detect statistically significant differences in the probabilities of a large number of patterns (the number of patterns increases as $L!$). Another drawback of the ordinal method is that it can lead to false conclusions when dealing with time series that contain many numbers that are equal [29], as it occurs when the spikes are perfectly locked to the modulation and the ISIs are very similar (equal to 2 or 3 modulation periods). In contrast, the Fano factor allows us to uncover long-range correlations in the ISI sequence.

This paper is organized as follows. Section 2 presents the experimental setup, the LK model, and the method used to quantify the spike timing regularity; in Sec. 3 we compare the results obtained from experimental and simulated spike sequences, and in Sec. 4, we present the discussion and our conclusions.

2. Methods

2.1. Experimental setup and data sets

The experimental setup was described in [19,22]. It consists of a semiconductor laser with optical feedback from an external cavity of 70 cm, which gives a feedback delay of 4.7 ns. The threshold current of the free-running laser is $I_{th,sol} = 26.62$ mA; with feedback it is $I_{th} = 24.70$ mA (7.2% reduction). A bias-tee was used to combine a constant dc current, I_{dc}, with a periodic signal from a function generator. Without the periodic signal the spike timing is irregular and I_{dc} controls the average spike rate, which varies from few to tens of MHz.

In the experiments three modulation parameters were varied, the dc value of the laser current, I_{dc}, the amplitude, A_{mod}, and frequency, f_{mod}, of the driving signal, and for each set of parameters, three modulation waveforms were used (pulse-down, pulse-up and sinusoidal). Time traces of the laser intensity were recorded with 10^7 data points with 0.5 ns resolution, covering a time interval of 5 ms. Here, we analyze the experimental data recorded with sinusoidal modulation and keeping fixed I_{dc}; we select a dc level for which the laser emits well-defined spikes: I_{dc}=26 mA. The intensity time traces contain about 9000–120000 power dropouts (spikes), depending on A_{mod} and f_{mod} [30].

2.2. Fano factor analysis

The Fano factor [31] is a measure that quantifies the regularity of a sequence of events. To calculate the Fano factor, F, we divide the intensity time trace in N_{int} non-superposing segments of duration T_{int} and count the number of spikes that occur in each segment (see Fig. 1); then, F is calculated as

$$F = \sigma^2(N_i)/\langle N_i \rangle. \tag{1}$$

where $\sigma^2(N_i)$ and $\langle N_i \rangle$ are the variance and the mean of the sequence of counts, $\{N_i\}$ with $i = 1, \ldots N_{int}$.

F is a function of the duration of the counting interval, T_{int}. If the spikes are generated by a fully random, homogeneous Poisson point process, the probability that N spikes occur in the interval T_{int} is $p(N, T_{int}) = (\lambda T_{int})^N \exp(-\lambda T_{int})/N!$ where λ is the average number of spikes per unit time (i.e., the spike rate). For this distribution $\sigma^2(N_i) = \langle N_i \rangle = \lambda T_{int}$ and thus, $F = 1 \, \forall \, T_{int}$ [32]. On the other hand, if the spikes are not fully random, F can take higher or lower values.
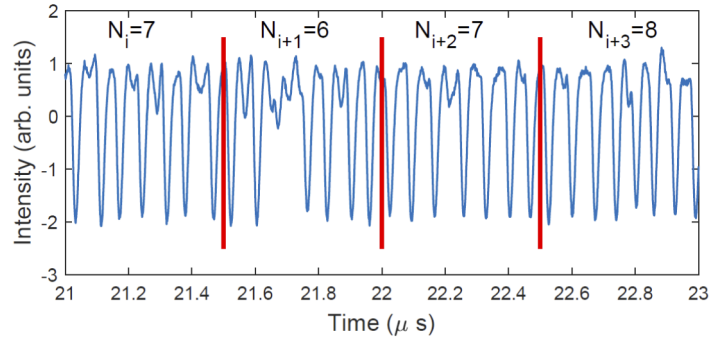
Fig. 1. The time series of the normalized relative intensity (which has zero mean and unit variance) is reduced to a sequence of counts $\{\ldots N_i, N_{i+1}, N_{i+2} \ldots\}$, by counting the number of spikes in successive intervals of duration T_{int} (here $T_{\text{int}} = 0.5\mu s$).

When the spikes are emitted with regular periodicity and T_{int} contains an integer number of periods, the variance of $\{N_i\}$ is low and F takes low values. In contrast, if the spikes are emitted in bursts (i.e., there are "silent" intervals with no or few spikes), the variance of $\{N_i\}$ is high, and F takes high values.

If the duration of the counting interval, T_{int}, is very small, then the sequence of counts becomes a sequence of 0s and 1s because in each interval there will be either 0 or 1 spike. Therefore, N_i is a random variable which takes the value 1 with probability p and the value 0 with probability $1 - p$. Since the variance of the Bernoulli distribution is $p(1 - p)$, when $T_{\text{int}} \to 0$, $p \to 0$ and $F \to 1$ [32].

2.3. Lang-Kobayashi model

The Lang-Kobayashi equations describing a single-mode semiconductor laser with weak optical feedback are [24]:

$$\dot{E} = k(1 + i\alpha)(G - 1)E + \eta E(t - \tau)e^{-i\omega_0\tau} + \sqrt{D}\xi, \tag{2}$$

$$\dot{N} = \gamma_N(\mu - N - G|E|^2). \tag{3}$$

Here E represents the slowly varying complex optical field and N represents the carrier density. η, τ, and $\omega_0\tau$ are the feedback strength, delay and phase respectively. α is the linewidth enhancement factor, $k = 1/(2\tau_p)$ where τ_p is the photon lifetime, $\gamma_N = 1/\tau_N$ where τ_N is the carrier lifetime, $G = N/(1 + \epsilon|E|^2)$ is the gain where ϵ is the gain saturation coefficient. μ is the pump current parameter that is sinusoidally modulated, $\mu(t) = \mu_{dc} + a_{mod}\sin(2\pi f_{mod}t)$ where μ_{dc}, a_{mod} and f_{mod} are the dc value, the amplitude and the frequency of the modulation. Spontaneous emission is represented by a complex additive Gaussian white noise, ξ, with strength D.

The equations were integrated with the following (typical) parameters that fit the experimental conditions: $k = 300$ ns^{-1}, $\gamma_N = 1$ ns^{-1}, $\alpha = 4$, $\epsilon = 0.01$, η=30 ns^{-1}, $\tau = 5$ ns, $\mu_{dc} = 0.99$, $D = 10^{-5}$ ns^{-2}. For these parameters the "natural" spike rate (without current modulation) is ~ 3.3 MHz, which is as that observed in the experiments with $I_{dc} = 26$ mA. We note that we use a value of μ_{dc} below the solitary threshold ($\mu_{th,sol} = 1$) because in the experiments $I_{th,sol} = 26.62$ mA (the influence of the dc value of the pump current was studied in [33], where we found a good agreement between experiments and model simulations).

The Euler-Maruyama method with an integration step of $dt = 1$ ps was used to integrate the equations. To detect the spike times the intensity time series, $|E(t)|^2$, was averaged over a smoothing window to simulate the 1 GHz bandwidth of the experimental detection system (a smooth digital bandpass filter [34] with cutoff frequencies 0 and 50 MHz was used), and then it

was normalized to zero mean and unit variance. Then, a spike was detected when the intensity decreased below a threshold, $Th = -1.1$ [25].

3. Results

We begin by examining the role of the modulation amplitude. Figure 2 displays the experimental distribution of inter-spike-intervals (ISIs) in log color scale, as a function of the modulation frequency, for various modulation amplitudes. The peak-to-peak modulation amplitude varies from 0.19 mA (top-left panel) to 0.631 mA (bottom-right panel) in steps of 0.063 mA. Since the dc value of the pump current is 26 mA, the modulation produces a variation of the pump current between 0.73% and 2.43%.
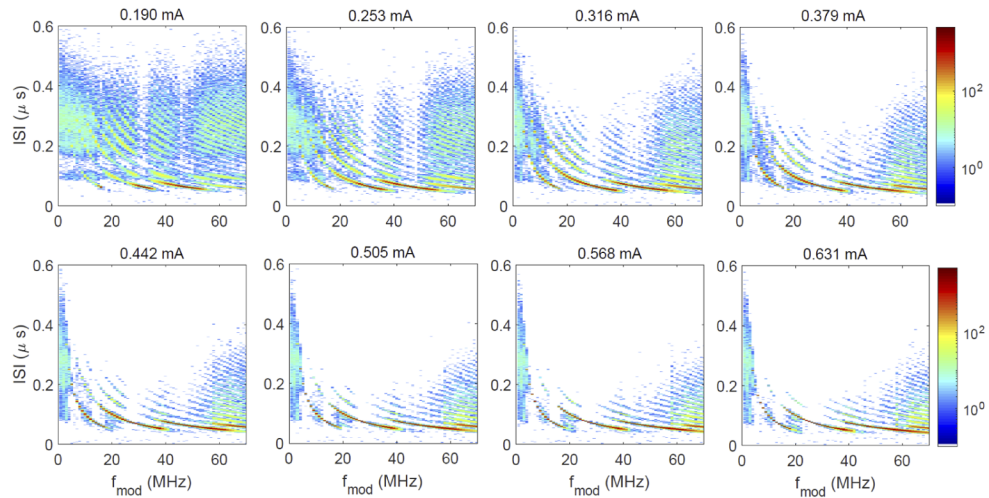

Fig. 2. Experimental distribution of inter-spike intervals (ISIs), the color code indicates the number of counts, the modulation amplitude is indicated in each panel.

We see that for the smaller modulation amplitude (top-left panel) the ISI distribution is broad (as expected because, without modulation, the spikes occur at irregular times). When the modulation frequency is low the distribution has no structure, but as the modulation frequency increases, a structure of well-defined peaks emerges. In particular intervals of the modulation frequency, f_{mod} ~30 MHz and 50 MHz, the ISI distribution becomes quite narrow. In these intervals the mean ISI is ~0.065 μs and thus, for $f_{mod} = 30$ MHz, $\langle ISI \rangle \times f_{mod} \sim 2$, while for 50 MHz, $\langle ISI \rangle \times f_{mod} \sim 3$. Therefore, for these modulation frequencies, a spike occurs every 2 or 3 modulation cycles.

The ISI distributions obtained from simulations of the LK model are presented in Fig. 3. In general, we see in general a good qualitative agreement with the experimental distributions. However, in the experimental ISI distribution we note that, for modulation amplitudes larger than 0.4 mA (second row in Fig. 2), at low modulation frequencies there is an abrupt variation in the shape of the ISI distribution, that becomes quite narrow for $f_{mod} \geq 5$ MHz; in contrast, in the simulated ISI distribution, Fig. 3, the is no abrupt change and the distribution gradually becomes narrower with increasing f_{mod}. In the simulations, for high enough modulation amplitude (bottom row in Fig. 3) the regions of subharmonic locking become narrow and even disappear. As we reported in [25], locking occurs within a limited range of modulation amplitudes. In Fig. 4 we consider a modulation frequency that produces 3:1 locking (in the left column, we present the simulated intensity; in the right column, the experimentally recorded intensity) and we can see

that, without modulation, or when the modulation amplitude is too small or too large (first row, second row and bottom row), the spike timing is irregular.
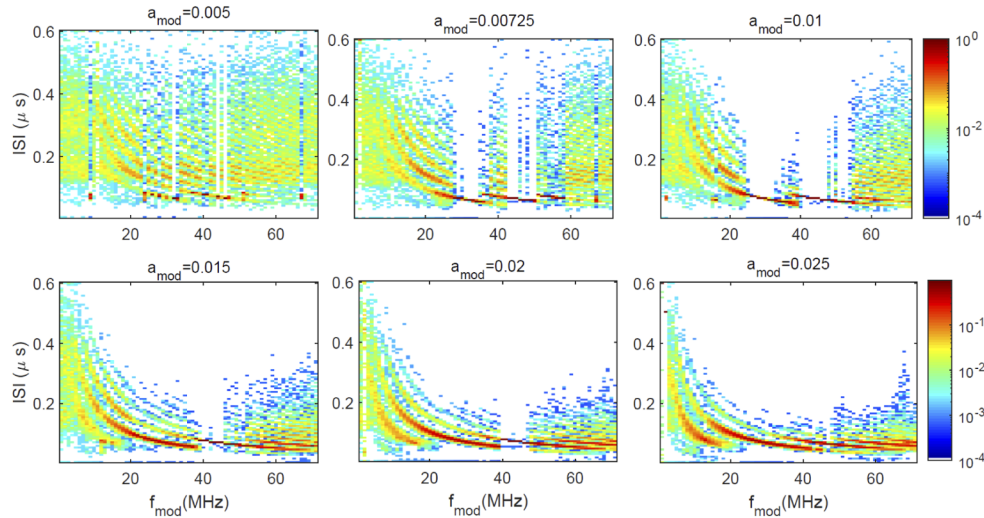

Fig. 3. ISI distribution calculated from simulated spike sequences. The modulation amplitude is indicated in each panel, other model parameter are indicated in the text.
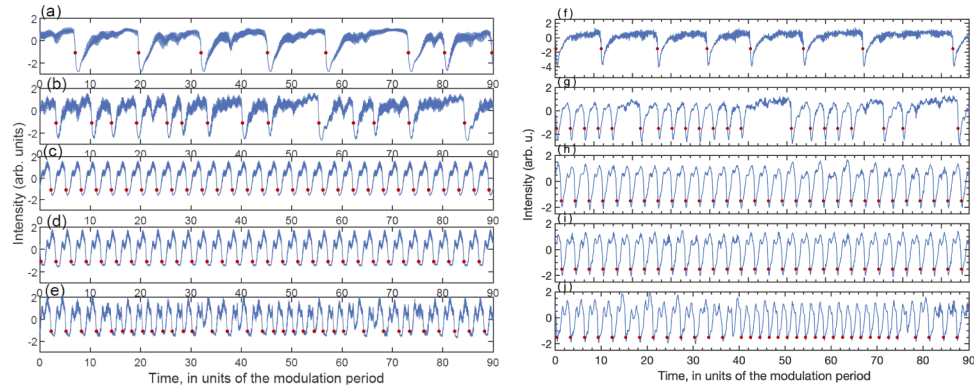

Fig. 4. Time series of the normalized relative intensity (a-e) simulated with the LK model and (f-j) experimentally recorded. In both cases, $f_{mod} = 42$ MHz. In the simulations $a_{mod} = 0$ (a), 0.008 (b), 0.0125 (c), 0.02 (d), 0.025 (e); in the experiments, 0 mA (a), 0.190 mA (b), 0.316 mA (c), 0.442 mA (d), 0.631 mA (e). The red dots indicate the detected spike times.

To further compare experiments and LK model simulations, we present in Fig. 5 the mean value of the ISI distribution and the coefficient of variation ($\sigma/\langle ISI \rangle$), for a modulation amplitude that produces two well-defined regions of sub-harmonic locking (in these regions, $\langle ISI \rangle \times f_{mod} = 2$ or 3). In the experiments the modulation amplitude, 0.631 mA, represents 2.4% of I_{dc} (I_{dc}=26 mA) while in the simulations, $a_{mod} = 0.025$ represents 2.5% of μ_{dc} ($\mu_{dc} = 0.99$). We again see a good qualitative agreement in the variation of $\langle ISI \rangle$ and $\sigma/\langle ISI \rangle$ with the modulation frequency.

While the above analysis confirms a qualitative similar variation of the ISI distribution, in the experiments and in the simulations, with the modulation amplitude and frequency, there might be differences in the timing of the spikes that can not be unveiled by the analysis of the ISI distribution. This is because the ISI distribution remains unchanged if we randomly shuffle the
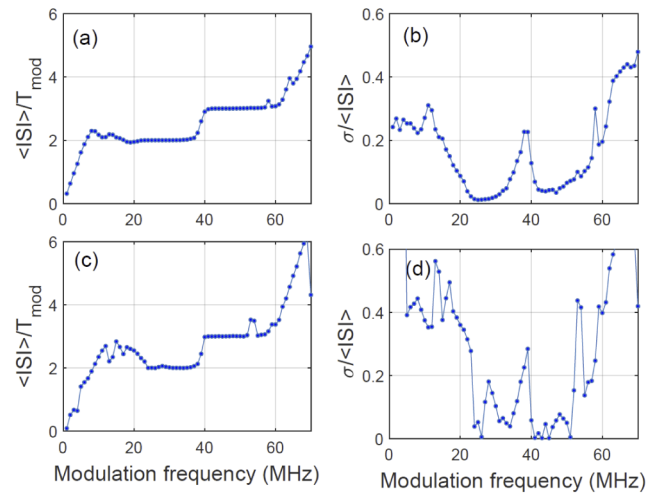
Fig. 5. Mean ISI in units of the modulation period (a, c) and coefficient of variation of the ISI distribution (b, d) vs. the modulation frequency, calculated from experimental spike sequences (a, b, the modulation amplitude is 0.631 mA) and from simulated spike sequences (c, d, $a_{mod} = 0.0125$).

ISIs (i.e., the analysis of the ISI distribution does not provide information about temporal order in the sequence of ISIs).

Therefore, to precisely compare the regularity of the spike times, we compare the Fano factor. The results are presented in Fig. 6 where we plot in log-log scale the Fano factor vs. the duration of the counting interval (in units of the modulation period), for different modulation frequencies indicated in color code. We see, as expected, that when $T_{\text{int}} \rightarrow 0$, $F \rightarrow 1$. On the other hand, when T_{int} contains a large number of modulation cycles, F can take large or small values, depending on the modulation frequency (the variation of F with f_{mod} was analyzed in [35]).
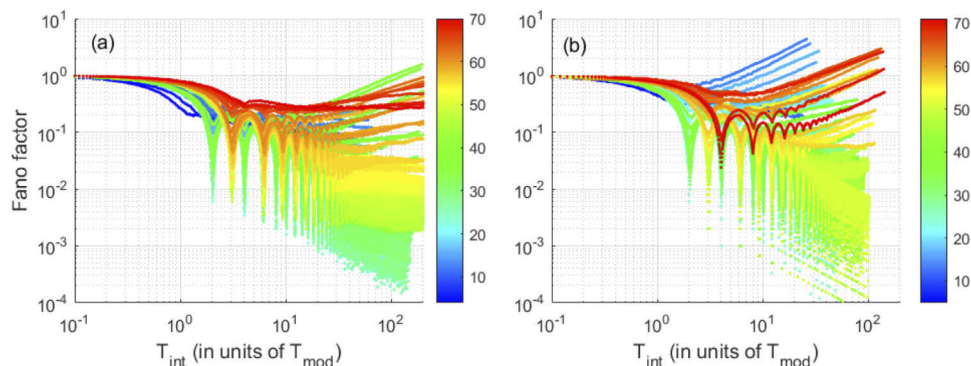

Fig. 6. Fano factor, F, vs. the duration of the spike counting interval, in units of the modulation period, calculated from experimental (a) and simulated (b) spike sequences. In both panels the color code indicates the modulation frequency in MHz, the modulation amplitudes are as in Fig. 5.

Let us consider the particular modulation frequencies that generate 2:1 and 3:1 locked spikes with most regular timing, i.e., with lowest coefficient of variation of the ISI distribution, $\sigma/\langle ISI \rangle$. As seen in Fig. 5(b) and (d), in both, experimental and simulated spike sequences $\sigma/\langle ISI \rangle$ is very

small when the modulation frequency is 26 MHz (2:1 locking) or 44 MHz (3:1 locking). For these modulation frequencies, the variation of F with T_{int} is shown in Fig. 7, where we again see a good qualitative agreement experiments–simulations. We see that F dips sharply whenever the spike counting interval contains an integer number of modulation cycles ($T_{\text{int}} = nT_{\text{mod}}$). In Fig. 7 panels (a) and (c) the modulation generates 2:1 locked spikes and the dips occur for $n = 2, 4, 6 \ldots$, while in panels (b) and (d), the modulation generates 3:1 locked spikes and the dips occur for $n = 3, 6, 9 \ldots$. In both cases, the dips persist for large n, revealing the long-range regularity of the spike timing.
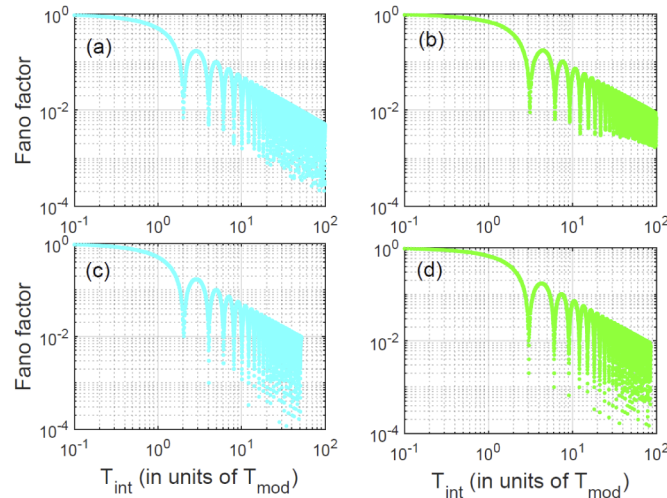

Fig. 7. Fano factor, F, vs. the duration of the spike counting interval (in units of the modulation period) calculated from experimental spikes sequences (a, b) and from simulated spikes sequences (c, d). In (a, c) the modulation, of frequency 26 MHz, generates 2:1 locked spikes (note that the first dip occurs when $T_{\text{int}} = 2T_{mod}$); in (b, d) the modulation, of frequency 44 MHz, generates 3:1 locked spikes (the first dip occurs when $T_{\text{int}} = 3T_{mod}$). The color code and other parameters are as in Fig. 6.

4.   Discussion and conclusions

To summarize, we have studied the regularity of the timing of the spikes in the output intensity of a semiconductor laser with optical feedback, operated in the LFF regime, and subject to a small-amplitude sinusoidal modulation of the laser current. We have performed a detailed comparison between experimental observations and simulations of the LK model, and found a good qualitative agreement. While it is well-known that the LK model reproduces the statistical characteristics of the LFFs, in terms of the shape of the ISI distribution and its variation with various parameters, the analysis of the ISI distribution is limited because it does not reveal the presence of temporal order in the ISI sequence (this is because if the ISIs are randomly shuffled, the ISI distribution does not change).

Using the Fano factor we have found a good qualitative agreement experiments-simulations. In particular, we have found that for modulation frequencies that generate subharmonically locked spikes, the spike timing regularity is long, as revealed by small values of the Fano factor calculated using long counting intervals. While we have previously found, using symbolic ordinal analysis, short-range correlations in the spike times, the Fano factor has allowed us to uncover long range correlations, that, when the spikes are subharmonically locked to the modulation, render the spike timing extremely regular. This regularity is surprising because in the experiments, the laser

operates below the solitary threshold, and thus, it is strongly influenced by noise, while in the LK model, noise also plays an important role because it may sustain the LFF dynamics. This is due to the fact that, in deterministic simulations, depending on the model's parameters, the spikes can be a transient dynamics towards stable emission [36,37].

For future work, it will be interesting to further understand the role of noise in the regularity of the spike timing. The interplay of noise and small-amplitude modulation can lead to enhanced regularity (a phenomenon known as stochastic resonance [17,38]). The regularity enhancement has usually been quantified by a narrowing of the ISI distribution, or by a narrowing of the main peak of the Fourier spectrum. The Fano factor, being a nonlinear measure based on counting the number of spikes occurring in consecutive segments of the intensity time series, can provide a new perspective on the interplay of noise, periodic modulation and time-delayed feedback, and can uncover new resonance phenomena. It will also be interesting to study how the refractory period (i.e., the recovery time after a power dropout) depends on the modulation amplitude and frequency, and how it affects the regularity of the spike timing.

Disclosures. The authors declare no conflicts of interest.

Data availability. The experimental sequences of inter-spike-intervals can be found in Ref. [30].

References

1. T. Erneux and P. Glorieux, *Laser Dynamics*, Cambridge University Press, Cambridge, 2010.
2. J. Ohtsubo, *Semiconductor Lasers: Stability, Instability and Chaos*, 4th ed., Springer, Berlin, 2017.
3. J. Sacher, D. Baums, P. Panknin, W. Elsasser, and E. O. Gobel, "Intensity instabilities of semiconductor lasers under current modulation, external light injection and delayed feeddback," Phys. Rev. A **45**(3), 1893–1905 (1992).
4. Y. Takiguchi, Y. Liu, and J. Ohtsubo, "Low-frequency fluctuation induced by injection-current modulation in semiconductor lasers with optical feedback," Opt. Lett. **23**(17), 1369 (1998).
5. S. F. Yu, "Nonlinear dynamics of vertical-cavity surface-emitting lasers," IEEE J. Quantum Electron. **35**(3), 332–341 (1999).
6. Y. Hong, S. Bandyopadhyay, and K. A. Shore, "Spectral signatures of the dynamics of current-modulated vertical-cavity surface-emitting lasers subject to optical feedback," J. Opt. Soc. Am. B **22**(11), 2350 (2005).
7. J. P. Toomey, D. M. Kane, M. W. Lee, and K. A. Shore, "Nonlinear dynamics of semiconductor lasers with feedback and modulation," Opt. Express **18**(16), 16955 (2010).
8. M. Sciamanna and K. A. Shore, "Physics and applications of laser diode chaos," Nat. Photonics **9**(3), 151–162 (2015).
9. S. Holzinger, C. Redlich, B. Lingnau, M. Schmidt, M. von Helversen, J. Beyer, C. Schneider, M. Kamp, S. Hofling, K. Ludge, X. Porte, and S. Reitzenstein, "Tailoring the mode-switching dynamics in quantum-dot micropillar lasers via time-delayed optical feedback," Opt. Express **26**(17), 22457 (2018).
10. O. Spitz, J. G. Wu, M. Carras, C. W. Wong, and F. Grillot, "Chaotic optical power dropouts driven by low frequency bias forcing in a mid-infrared quantum cascade laser," Sci. Rep. **9**(1), 4451 (2019).
11. O. Spitz, J. G. Wu, A. Herdt, M. Carras, W. Elsasser, C. W. Wong, and F. Grillot, "Investigation of chaotic and spiking dynamics in mid-infrared quantum cascade lasers operating continuous-waves and under current modulation," IEEE J. Sel. Top. Quantum Electron. **25**(6), 1200311 (2019).
12. A. V. Kovalev, M. S. Islam, A. Locquet, D. S. Citrin, E. A. Viktorov, and T. Erneux, "Resonances between fundamental frequencies for lasers with large delayed feedbacks," Phys. Rev. E **99**(6), 062219 (2019).
13. S. A. Zibrov, D. S. Chuchelov, A. E. Drakin, D. A. Shiryaev, E. A. Tsygankov, M. I. Vaskovskaya, V. V. Vassiliev, V. L. Velichansky, and A. P. Bogatov, "Modulation properties of an extended cavity diode laser and dynamic mode splitting," IEEE J. Quantum Electron. **56**(3), 1–7 (2020).
14. D. W. Sukow and D. J. Gauthier, "Entraining power-dropout events in an external-cavity semiconductor laser using weak modulation of the injection current," IEEE J. Quantum Electron. **36**(2), 175–183 (2000).
15. J. M. Mendez, R. Laje, M. Giudici, J. Aliaga, and G. B. Mindlin, "Dynamics of periodically forced semiconductor laser with optical feedback," Phys. Rev. E **63**(6), 066218 (2001).
16. J. S. Lawrence and D. M. Kane, "Nonlinear dynamics of a laser diode with optical feedback systems subject to modulation," IEEE J. Quantum Electron. **38**(2), 185–192 (2002).
17. F. Marino, M. Giudici, S. Barland, and S. Balle, "Experimental evidence of stochastic resonance in an excitable optical system," Phys. Rev. Lett. **88**(4), 040601 (2002).
18. W.-S. Lam, P. N. Guzdar, and R. Roy, "Effect of spontaneous emission noise and modulation on semiconductor lasers near threshold with optical feedback," Int. J. Mod. Phys. B **17**(22n24), 4123–4138 (2003).

19. A. Aragoneses, T. Sorrentino, S. Perrone, D. J. Gauthier, M. C. Torrent, and C. Masoller, "Experimental and numerical study of the symbolic dynamics of a modulated external-cavity semiconductor laser," Opt. Express **22**(4), 4705 (2014).

20. T. Sorrentino, C. Quintero-Quiroz, A. Aragoneses, M. C. Torrent, and C. Masoller, "Effects of periodic forcing on the temporally correlated spikes of a semiconductor laser with feedback," Opt. Express **23**(5), 5571 (2015).

21. T. Sorrentino, C. Quintero-Quiroz, M. C. Torrent, and C. Masoller, "Analysis of the spike rate and spike correlations in modulated semiconductor lasers with optical feedback," IEEE J. Sel. Top. Quantum Electron. **21**(6), 561–567 (2015).

22. J. Tiana-Alsina, C. Quintero-Quiroz, M. Panozzo, M. C. Torrent, and C. Masoller, "Experimental study of modulation waveforms for entraining the spikes emitted by a semiconductor laser with optical feedback," Opt. Express **26**(7), 9298 (2018).

23. J. Tiana-Alsina, C. Quintero-Quiroz, and C. Masoller, "Comparing the dynamics of periodically forced lasers and neurons," New J. Phys. **21**(10), 103039 (2019).

24. R. Lang and K. Kobayashi, "External optical feedback effects on semiconductor injection-laser properties," IEEE J. Quantum Electron. **16**(3), 347–355 (1980).

25. J. Tiana-Alsina and C. Masoller, "Locking Phenomena in semiconductor lasers near threshold with optical feedback and sinusoidal current modulation," Appl. Sci. **11**(17), 7871 (2021).

26. C. Bandt and B. Pompe, "Permutation entropy: a natural complexity measure for time series," Phys. Rev. Lett. **88**(17), 174102 (2002).

27. M. C. Soriano, L. Zunino, O. A. Rosso, I. Fischer, and C. R. Mirasso, "Time scales of a chaotic semiconductor laser with optical feedback under the lens of a permutation information analysis," IEEE J. Quantum Electron. **47**(2), 252–261 (2011).

28. J. P. Toomey and D. M. Kane, "Mapping the dynamic complexity of a semiconductor laser with optical feedback using permutation entropy," Opt. Express **22**(2), 1713 (2014).

29. L. Zunino, F. Olivares, F. Scholkmannd, and O. A. Rosso, "Permutation entropy based time series analysis: Equalities in the input signal can lead to false conclusions," Phys. Lett. A **381**(22), 1883–1892 (2017).

30. J. Tiana-Alsina and C. Masoller, "Inter-spike Intervals Data," Zenodo (2022), https://doi.org/10.5281/zenodo.5913506.

31. U. Fano, "Ionization yield of radiations. II. The fluctuations of the number of ions," Phys. Rev. **72**(1), 26–29 (1947).

32. M. C. Teich, C. Heneghan, S. B. Lowen, T. Ozaki, and E. Kaplan, "Fractal character of the neural spike train in the visual system of the cat," J. Opt. Soc. Am. A **14**(3), 529 (1997).

33. J. Tiana-Alsina and C. Masoller, "Experimental and numerical study of locking of low frequency fluctuations of a semiconductor laser with optical feedback," submitted (2022).

34. W. H. Press, S. A. Teukolsky, W. T. Vetterling, and B. P. Flannery, *Numerical Recipes*, Sec. 13.5 (Cambridge University Press 1992).

35. J. Tiana-Alsina and C. Masoller, "Time crystal dynamics in a weakly modulated stochastic time delayed system," submitted (2022).

36. A. Torcini, S. Barland, G. Giacomelli, and F. Marin, "Low-frequency fluctuations in vertical cavity lasers: Experiments versus Lang-Kobayashi dynamics," Phys. Rev. A **74**(6), 063801 (2006).

37. J. Zamora-Munt, C. Masoller, and J. Garcia-Ojalvo, "Transient low-frequency fluctuations in semiconductor lasers with optical feedback," Phys. Rev. A: At., Mol., Opt. Phys. **81**(3), 033820 (2010).

38. S. Barbay, G. Giacomelli, and F. Marin, "Stochastic resonance in vertical cavity surface emitting lasers," Phys. Rev. E **61**(1), 157–166 (2000).